



# Influence of reservoir lithology on porous flow resistance of gas-bearing tight oil reservoirs and production forecast

Yuan Rao<sup>1,2</sup> · Zhengming Yang<sup>2,3</sup> · Lijing Chang<sup>4</sup> · Yapu Zhang<sup>2,3</sup> · Zhenkai Wu<sup>1,2</sup> · Haibo Li<sup>2,3</sup>

Received: 16 August 2021 / Accepted: 26 October 2021 / Published online: 8 November 2021  
© The Author(s) 2021

## Abstract

The release of dissolved gas during the development of gas-bearing tight oil reservoirs has a great influence on the effect of development. In this article, the high-pressure mercury intrusion experiment was carried out in cores from different regions and lithologies of the Ordos Basin and the Sichuan Basin. The objectives are to study the microscopic characteristics of the porous throat structure of these reservoirs and to analyze the porous flow resistance laws of different lithology by conducting a resistance gradient test experiment. A mathematical model is established and the oil production index is corrected according to the experiment results to predict the oil production. The experimental results show that for tight reservoirs in the same area and lithology, the lower the permeability under the same back pressure, the greater the resistance gradient. And for sandstone reservoirs in different areas, the resistance gradients have little difference and the changes in the resistance coefficients are similar. However, limestone under the same conditions supports a much higher resistance gradient than sandstone reservoirs. Furthermore, the experimental results are consistent with the theoretical analysis indicating that the PVT (pressure–volume–temperature) characteristics in the nanoscale pores are different from those measured in the high-temperature, high-pressure sampler. Only when the pressure is less than a certain value of the bubble point pressure, the dissolved gas will begin to separate and generate resistance. This pressure is lower than the bubble point pressure measured in the high-temperature and pressure sampler. The calculation results show that the heterogeneity of limestone reservoirs and the mismatch of fluid storage and flow space will make the resistance, generated by the separation of dissolved gas, have a greater impact on oil production.

**Keywords** Gas-bearing tight oil · Resistance gradient · Tight sandstone · Tight limestone · Material balance · Production forecast

## Introduction

Tight oil reservoir is a trendy topic for exploration and development as a typical unconventional petroleum resource (Zhou et al. 2021; Zhu et al. 2019; Annual Energy Outlook 2020; Ali et al. 2020). The technically recoverable resources

of tight oil in China are predicted to be about  $(20\text{--}25) \times 10^8$  t, which is an important replacement resource (Song et al. 2020a; Qin et al. 2021; Gao et al. 2021). Tight oil is light in quality and contains dissolved gas. Some tight oil reservoirs even have high original gas–oil ratio. The most typical ones are Triassic tight sandstone in Ordos Basin and Jurassic tight sandstone and tight limestone in Mid-Sichuan Basin, as shown in Fig. 1.

Pressure of formation drops quickly by means of depletion-drive mechanism, which is the main exploitation method of tight reservoirs due to difficulty to replenish energy caused by small pore throats. When pressure drops to bubble point pressure, dissolved gas begins to separate out, which leads to a sharp decline in production and seriously affects the effectiveness of tight oil development (Shen et al. 2021; Wu et al. 2014; Xiao et al. 2018; Jones 2016). Hence, research on porous flow resistance of tight oil reservoirs is

✉ Yuan Rao  
raoyuan171@mails.ucas.edu.cn

<sup>1</sup> College of Engineering Science, University of Chinese Academy of Sciences, Beijing 100049, China

<sup>2</sup> Institute of Porous Flow and Fluid Mechanics, University of Chinese Academy of Sciences, Langfang 065007, China

<sup>3</sup> Research Institute of Petroleum Exploration and Development, Beijing 100083, China

<sup>4</sup> Oil and Gas Technology Research Institute Changqing Oilfield Company, Xi'an 710021, China

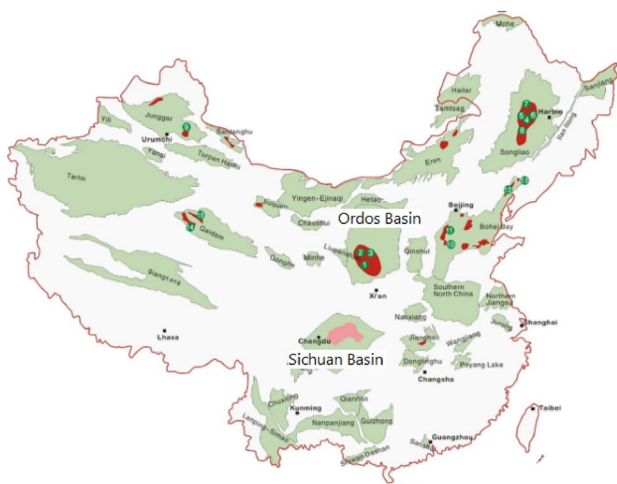


**Fig. 1** Location of Ordos basin and Sichuan basin (Guo et al. 2018)

of great significance to effectively develop tight reservoirs. Current experimental study on depletion-drive mechanism of gas-bearing oil reservoirs is mainly divided into microscopic visualization study and macroscopic depressurization experiment simulating depletion-drive process. Chatenever (Chatenever et al. 1959) first studied degassing process of gas-bearing oil reservoirs through microscopic visualization experiment and described characteristics of gas phase changes in porous media during degassing. Later, many scholars also used glass etching model and other visual methods to observe phase change process of gas-bearing oil in porous media (Bora et al. 2000; Danesh et al. 1987; Lago et al. 2002; Dominguez et al. 2000). Based on these perceptual understandings, scholars in China and abroad have performed depressurization experiments to simulate depletion-drive process through sand packs and cylindrical cores, as well as studied the influence of factors such as pressure drop rate, back pressure, and oil viscosity on oil production and production gas–oil ratio. Internal mechanism of the influence is analyzed combining with the results obtained from microscopic experiments (Lu et al. 2016; Akin and Kovscek 2002; Sheikha and Darvish 2012; Arora and Kovscek 2003; Moulu 1989; Stewart et al. 1954; Zhang et al. 2018). Current experimental studies mainly focus on mid-high permeability or heavy oil reservoirs, but few on tight oil. The porous flow pattern of heavy oil is very different from that of conventional oils, which mainly presents the form of foamy oil flow and has a unique pseudo-bubble point pressure (Smith 1988; Maini 1999; Abusahmin et al. 2017). Furthermore, the microstructure characteristics of mid-high permeability formation are very different from tight oil formation (Guo et al. 2020; Wang et al. 2020; Chen et al. 2018; Nithiwat et al. 2017; Yan et al. 2017). Hence, whether the conclusions drawn in mid-high permeability and heavy oil reservoirs can be applied to tight oil reservoirs needs further study. At the

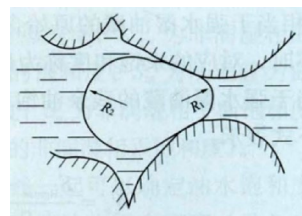


**Fig. 2** A sketch of Jamin effect

same time, the existing studies mainly focus on microscopic mechanism of porous flow, but few on porous flow resistance or the influence of different lithology on porous flow resistance. This paper focuses on tight oil reservoirs, uses physical simulation experiments and high-pressure mercury porosimeters to analyze the microscopic pore structure characteristics of cores with different lithology and permeability. It also establishes a test method to estimate the porous flow resistance gradient of gas-bearing in tight oil reservoirs and studies the impact of gas separation on production of tight oil reservoirs.

## Porous flow resistance experiment

### Principle

When production pressure is lower than bubble point pressure during development of gas-bearing tight oil reservoirs, dissolved gas in crude oil begins to separate out, and the separated gas produces additional resistance, which is called Jamin effect. Jamin Effect, a kind of interface effect, refers to the resistance caused by the deformation of separated gas passing through throats. As a consequence, the narrower the throats, the greater the resistance, as shown in Fig. 2. From the perspective of micro-mechanism, the definition of Jamin effect is Eq. (1). Resistance in gas-bearing tight reservoirs is higher due to the low permeability, the narrow throats and the Jamin effect. The latter make resistance extremely important, seriously affecting productivity and therefore must be considered in the development process.

$$p_c = 2\sigma \left( \frac{1}{R_1} - \frac{1}{R_2} \right) \quad (1)$$

Theoretically, the capillary force on each interface can be calculated by Eq. (1), but in practice, this is impossible. The reason is that we cannot know exactly how many interfaces are generated, as well as the radius of the throat corresponding to each interface. Besides, interfaces are always changing. So if we want to measure resistance quantitatively, we can only use a macro-method. In order to experimentally

and quantitatively characterize resistance of gas-bearing oil, the ratio of pressure difference between two ends of a core to core length is defined as resistance coefficient  $R$ , namely:

$$R = \frac{p_1 - p_2}{L} \quad (2)$$

where  $R$  is resistance gradient, MPa/m;  $p_1$  is final stable value of pressure at core inlet, MPa;  $p_2$  is back pressure at core outlet, MPa;  $L$  is core length, m.

In tight reservoirs, the size and distribution frequency of pore throats is an important factor affecting flow capacity of reservoirs (Li et al. 2020, 2017, 2018; Lin et al. 2021, 2018). In order to better analyze resistance of gas to cores with different lithology and permeability, microscopic pore throat structure characteristics are first studied using a high-pressure mercury porosimeter.

### Cores and fluids

Nine cores were selected for the experiment, including three tight sandstone cores from Triassic Yanchang Formation in Ordos Basin, three tight sandstone cores from Jurassic Shaximiao Formation in Sichuan Basin, and three tight limestone cores from Jurassic Da'anzhai Formation in Sichuan Basin. The diameter of each core is 2.5 cm, other parameters are shown in Table 1.

The oil for experiment is degassed crude oil uniformly selected from Ordos Basin to compound live oil in order to reduce the influence of other factors. Live oil is compounded by degassed crude oil and dissolved gas in a high-temperature and high-pressure sampler. Dissolved gas is prepared according to the main components of associated gas on site, which is composed of  $\text{CH}_4$ ,  $\text{C}_2\text{H}_6$ ,  $\text{C}_3\text{H}_8$  and  $\text{N}_2$ , with mole fractions of 54.8%, 37.0%, 5.0% and 3.2% separately. The dissolved gas–oil ratio is  $80\text{m}^3/\text{t}$ , the viscosity of degassed crude oil at reservoir temperature ( $72^\circ\text{C}$ ) is  $1.23\text{ mPa}\cdot\text{s}$ , and the live oil bubble point pressure is  $10.72\text{ MPa}$  measured

under formation conditions in high-temperature and pressure sampler. The formation water used is prepared with distilled water and  $\text{NaCl}$ ,  $\text{CaCl}_2$ ,  $\text{MgCl}_2$ , which occupy  $43.75\text{ g/L}$ ,  $3.75\text{ g/L}$  and  $2.50\text{ g/L}$ , respectively.

### Procedures

#### Characteristics of microscopic pore throat structure

High-pressure mercury injection technology is based on capillary model and uses non-wetting phase to replace wetting phase. During mercury injection, capillary radius corresponding to injection pressure is the throat radius, and the mercury injection value corresponds to the pore volume controlled by the throat. Capillary pressure curve and pore throat distribution curve can be obtained by constantly changing injection pressure. The minimum pore size tested by the porosimeter is  $2\text{ nm}$  (Yang et al. 2017). The instrument used in the experiment is PoreMaster@60/33 mercury intrusion meter from Kantar Corporation. The cores have been dried at  $105^\circ\text{C}$  to a constant weight before mercury intrusion.

#### Porous flow resistance gradient experiment

The experiment procedure is shown in Fig. 3, which includes three systems: gas-containing oil compounding system, displacing system and back pressure controlling system. The gas-containing oil compounding system includes a TC-100D constant speed and pressure pump, a high-temperature and pressure gas-containing oil sampler, and an intermediate container filled with kerosene. The displacing system includes a core holder, a confining pressure pump, inlet and outlet pressure sensors, a differential pressure sensor with accuracy of  $0.0015\text{ MPa}$ , computer and recording software. The back pressure control system includes a piston container

**Table 1** Parameters of cores

Core number	Porosity (%)	Gas log permeability (mD)	Lithology	Region
17-3B	9.35	0.08	Sandstone	Ordos
10-2A	10.48	0.27	Sandstone	Ordos
15-1B	13.23	0.59	Sandstone	Ordos
0218	2.61	0.003	Sandstone	Sichuan
0204	3.08	0.11	Sandstone	Sichuan
0322	4.77	0.94	Sandstone	Sichuan
119	1.51	0.03	Limestone	Sichuan
164	1.49	0.15	Limestone	Sichuan
139	2.25	0.65	Limestone	Sichuan

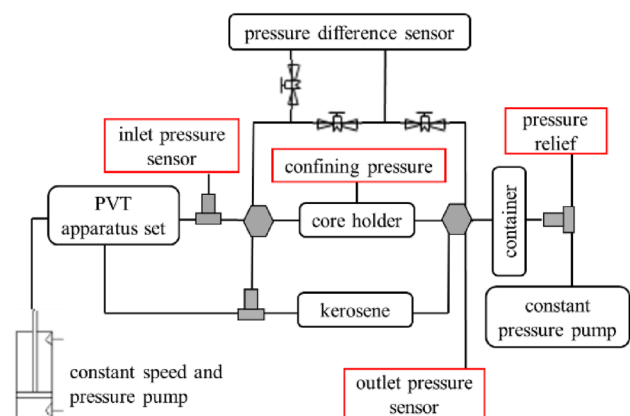


**Fig. 3** Experimental scheme of pressure gradient experiment

filled with nitrogen and a confining pressure pump. The experiment is carried out in a thermostat.

The experiment steps are as follows:

1. Connect equipment according to Fig. 3, use constant speed and pressure pump to raise pressure in the back pressure intermediate container to 15 MPa;
2. Use kerosene to empty fluid in the core holder and pipeline without confining pressure, then raise pressure in pipeline at both ends of the core holder to 16 MPa;
3. Add 18 MPa confining pressure, open valves between the core holder and the back pressure intermediate container, then use gas-bearing oil to displace the core under the constant pressure of 18 MPa. After the displacement of 10 times the pore volume, close the valves;
4. Open valves of the differential pressure transducer, and use computer software to record sensor reading every 1 min until pressure difference change is less than 0.15% in an hour;
5. Reduce pressure in back pressure intermediate container regularly, repeat process ④ to obtain a stable value of pressure difference between the core at different back pressure, and calculate the resistance gradient coefficient  $R$  according to the definition formula (1).

## Experimental results

Figure 4 shows the test curve of the high-pressure mercury intrusion experiment of 9 cores. From the results, it can be seen that with increase in permeability, proportion of space occupied by wide throats increases while narrow throats' decreases, and the homogeneity of sandstone is strong, while that of limestone is weak. As shown in Figs. 5 and 6, sandstone cores have almost no space occupied by micron-scale throats wider than  $1\ \mu\text{m}$ , while the submicron-scale throats' accounts for the largest proportion with a relatively similar variation and strong homogeneity.

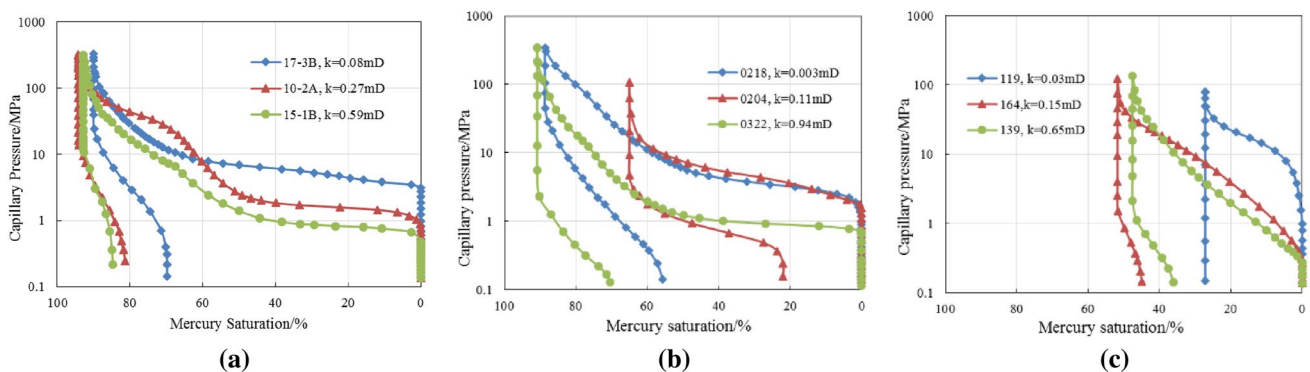


**Fig. 4** High-pressure mercury intrusion test curves of 9 cores. **a** 3 Ordos sandstone cores. **b** 3 Mid-Sichuan sandstone cores. **c** 3 Mid-Sichuan limestone cores

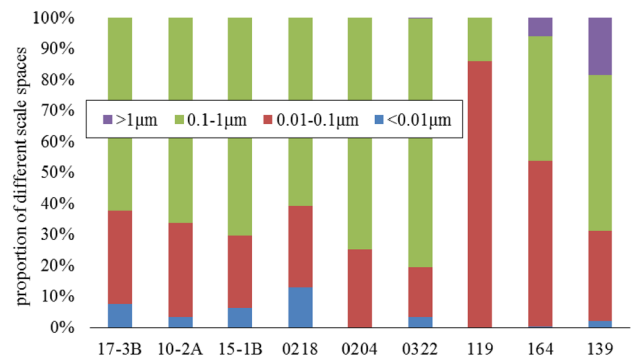


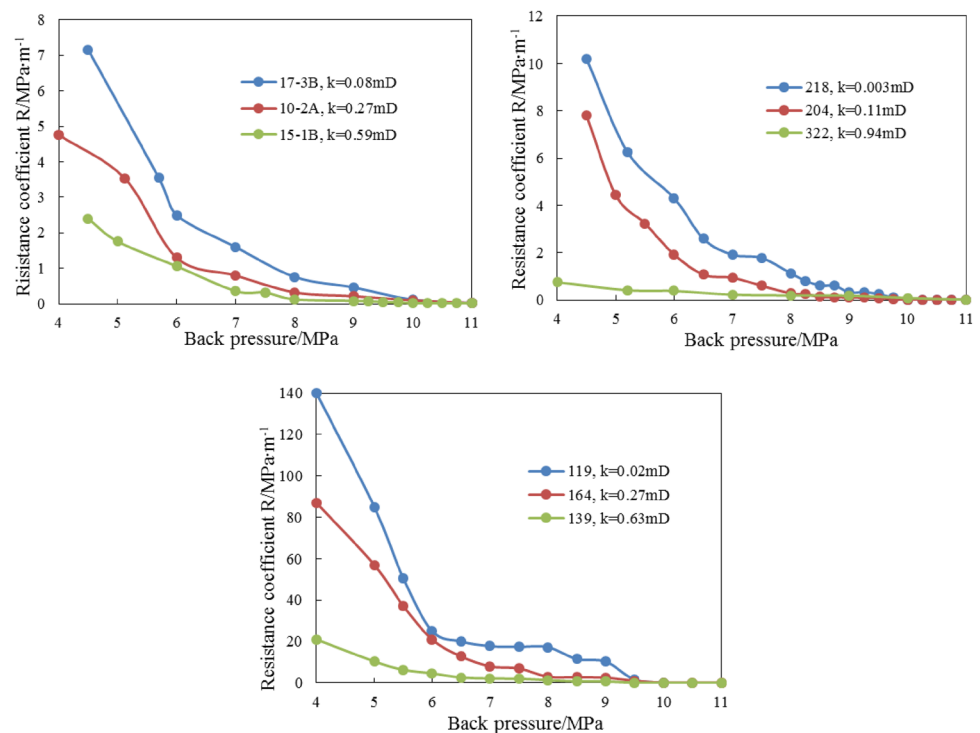
**Fig. 5** Proportion of different scale spaces

However for limestone, the space occupied by micron-scale throats can account for up to 18.3% when permeability is high, while the space occupied by nanoscale throats in the range of  $0.01\text{--}0.1\ \mu\text{m}$  also accounts for a large proportion, which can reach 86.1% when permeability is low. It shows that microstructure of sandstone formation in the two different regions is similar, both develop submicron-scale and nanoscale throats and almost no micron-scale throats. On the other hand, limestone has poor homogeneity and relatively narrow throats, and micro-nanoscale throats occupy a larger proportion, which is obviously different from sandstone.

Porous flow resistance gradient under different back pressures is calculated according to definition formula of resistance gradient  $R$ , the relationship between back pressure and resistance gradient of 9 cores is shown in Fig. 6. It can be seen from the figure that:

- (1) For cores with the same lithology in the same area, the lower the permeability under the same back pressure, the greater the resistance gradient. Taking Ordos tight sandstone as an example, when back pressure is 8 MPa, resistance gradient of core 17-3B is 0.762 MPa/m, of core 10-2A is 0.325 MPa/m, and of core 15-1B is

**Fig. 6** Relationship between back pressure and resistance gradient



0.129 MPa/m. This is because when back pressure is lower than bubble point pressure, there is a process of bubble nucleation and growth. When formation throats are narrow, the permeability is low and consequently a resistance to porous flow will be generated when tiny bubbles pass through them. When formation throats are wide, the permeability is high and tiny bubbles do not yet generate a resistance gradient. According to Jamin effect, when bubbles of the same size pass through throats of different sizes, the resistance gradients produced are different. The smaller the throat radius, the greater the resistance. Combined with the results of high-pressure mercury injection experiments, core 17-3B has a narrow throat, while core 10-2A and core 15-1B have wider throats and similar pore throat structures, so core 17-3B has the largest resistance gradient, and the other two have lower ones and not much difference.

- (2) For sandstone cores in two different regions, variation patterns of resistance are similar; for cores with different lithology, resistance of limestone under the same permeability and back pressure is much higher than that of sandstone. As shown in Fig. 7, resistance of sandstone increases exponentially as permeability decreases, and the order of magnitude is the same; while for sandstone and limestone cores with the same permeability and back pressure of 0.27mD and 8 MPa, the resistance coefficients could differ by up to 10 times, which shows that pore structure has a great

influence on resistance gradient. Combined with the results of high-pressure mercury intrusion experiment, for limestone formation, the percentage of micron- and submicron-scale pores has a tendency to increase as permeability increases, but the nanoscale pores still account for a large proportion. While the main contribution to permeability is derived from the micron- and submicron-scale pores, the fluid storage does not match the flow space, resulting in high resistance gradient (Wang et al. 2019; Qiao et al. 2020; Zhang et al. 2020). For sandstone formation, as permeability increases, the percentage of submicron pores increases. At the same time, permeability contribution mainly comes from submicron pores, the fluid storage space matches the flow space, so the resistance gradient is low.

- (3) When back pressure is lower than the bubble point pressure 10.72 MPa within a certain range, dissolved gas in cores is not separated out, which is an unique phenomenon of tight reservoirs. This is consistent with the theoretical analysis results in the literature (Zhang et al. 2002; Song et al. 2020b; Nojabaei et al. 2013), that is, the PVT (pressure–volume–temperature) characteristics in nanoscale pores are different from those measured in high-temperature and high-pressure sampler. Due to the narrow throat, capillary force is generated, which affects the phase change process, so pressure must drop to a lower value, then dissolved gas will separate out.

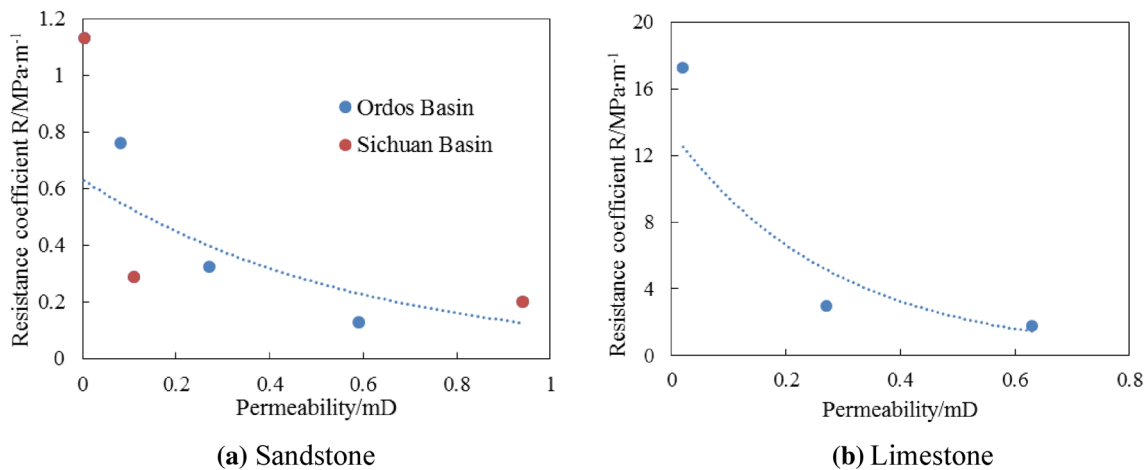


Fig. 7 Relationship between resistance coefficient and permeability of different lithology cores

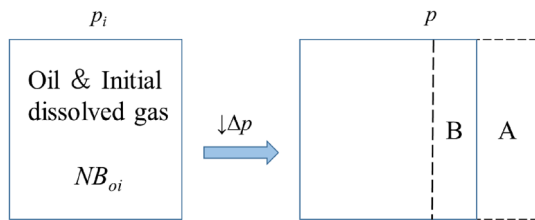


Fig. 8 Material balance model for gas-bearing tight oil reservoir

Hence, there is no porous flow resistance gradient yet in the initial stage of separation.

## Production forecast model

For oil reservoirs that have been put into development, dynamic reserves are one of the key indicators for evaluating development status. Dynamic reserves are the total volume of fluid that can finally flow effectively under current mining technology conditions. The material balance method is an effective and accurate method for calculating dynamic reserves. The existing material balance models for gas-bearing oil reservoirs are mostly established for conventional medium and high permeability reservoirs and usually do not consider the influence of the resistance gradient caused by the Jamin effect, so the results are quite different from the actual ones.

According to the results of the experiment in the previous section, the oil production index item in the model is revised, and the influence of dissolved gas resistance on production is considered to establish a more accurate mass balance production forecast model.

## Model establishment

The gas-bearing tight oil reservoir model is shown in Fig. 8. In the initial state, formation pressure is  $p_i$ , and the total volume of oil and original dissolved gas in reservoir is  $NB_{oi}$ ; when pressure is  $p$ , the pressure drops by  $\Delta p$ . At this time, original oil and dissolved gas volume changes are divided in two parts: A and B. A is the increased volume of oil and original dissolved gas due to expansion; B is the decrease in hydrocarbon-containing pore volume caused by the expansion of bound water and the decrease in pore volume.

For undersaturated oil reservoirs,  $p_i > p_b$ , the material balance equation is

$$N_E = NB_{oi} [C_f + \varphi (S_{oi} C_o + S_{wc} C_w)] \Delta p / B_{ob} \quad (3)$$

where  $N_E$  is elastic oil production,  $m^3$ ;  $N$  is original reserves of formation,  $m^3$ ;  $B_{oi}$  is formation oil volume factor under original formation pressure,  $m^3/m^3$ ;  $C_f$  is fracture compression factor,  $1/MPa$ ;  $\varphi$  is porosity, %;  $S_{oi}$  is original oil saturation;  $C_o$  is isothermal compression coefficient of formation oil,  $1/MPa$ ;  $S_{wc}$  is irreducible water saturation, %;  $C_w$  is isothermal compressibility coefficient of formation water,  $1/MPa$ ;  $B_{ob}$  is formation oil volume coefficient under bubble point pressure,  $m^3/m^3$ .

For saturated oil reservoirs,  $p_i < p_b$ , the material balance equation is

$$\begin{aligned} & N_p [B_o + B_g (R_p - R_s)] \\ &= N_m \left[ B_o - B_{ob} + B_g (R_{si} - R_s) + \frac{C_w S_{wm} + C_{fm} B_{ob} \Delta p}{1 - S_{wm}} \right] \\ &+ N_f \left[ B_o - B_{ob} + B_g (R_{si} - R_s) + \frac{C_w S_{wf} + C_{ff} B_{ob} \Delta p}{1 - S_{wf}} \right] \end{aligned} \quad (4)$$

where  $R_p$  is cumulative gas–oil ratio, ground cumulative gas production (ground  $m^3$ )/ground cumulative oil production (ground  $m^3$ );  $R_s$  is dissolved gas–oil ratio,  $m^3/m^3$ ;  $R_{si}$  is original dissolved gas–oil ratio,  $m^3/m^3$ ;  $N_m$  is original formation oil reserves in matrix system,  $m^3$ ;  $S_{wm}$  is formation water saturation in matrix system;  $C_{fm}$  is matrix compressibility;  $N_f$  is original formation oil reserves in fracture system,  $m^3$ ;  $N_p$  is cumulative oil production,  $m^3$ ;  $S_{wf}$  is formation water saturation in fracture system;  $C_{ff}$  is fracture compression factor.

The derived material balance equation considers the dual media model composed of matrix system and fracture system (it is a generalization of the model). The porosity of the two systems is calculated separately. The porosity of matrix system includes organic and inorganic matrix; the porosity of fracture system includes natural and artificial cracks.

### Model solution

According to the material balance finite difference method proposed by Aguilera (Orozco and Aguilera 2018), the change law of the recovery factor of reservoirs with time is predicted. The finite difference equation for pressure below bubble point is derived as follows:

$$\Delta N_p = \frac{\left[ N - (N_p)_i \right] \Delta \left( \frac{B_o}{B_g} - R_s \right) + N B_{ob} \left\{ [(1 - \omega)C' + \omega C''] \Delta p \left[ \Delta \left( \frac{1}{B_g} \right) + \left( \frac{1}{B_g} \right)_{i+1} \right] - \Delta \left( \frac{1}{B_g} \right) \right\}}{\left( \frac{B_o}{B_g} - R_s \right)_{i+1} + R_{avg}} \tag{5}$$

where  $R_{avg}$  is average value of  $R$  at step  $i$  and step  $i + 1$ ;  $B_g$  is volume factor of dissolved gas under formation conditions,  $m^3/(\text{standard})m^3$ ;  $\omega$  is proportion of fracture system in initial oil reserves.

The compressibility coefficients  $C'$  and  $C''$  of the matrix and the fracture systems are

$$t_{i+1} = t_i + \Delta t_{i+1} \tag{6}$$

$$C'' = \frac{C_w S_{wf} + C_f}{1 - S_{wf}} \tag{7}$$

The variable symbol  $\Delta$  in formulas represents the amount of change from step  $i$  to step  $i + 1$ . It is necessary to know all physical parameters in advance.

First, write a material balance equation only for matrix system, use the relative permeability data of matrix system, and calculate the relationship between oil saturation  $S_{om}$  and pressure of matrix system. This step is only necessary when oil and gas saturation of fracture system changes with time and pressure. If oil and gas phase saturation of fracture system are not considered, this step can be omitted.

Calculate total average irreducible water saturation of matrix system and fracture system in the initial state

$$S_{wi} = S_{wim}(1 - v_i) + S_{wif}v_i \tag{8}$$

where  $v$  is segmentation coefficient, which can be obtained from well test data;  $S_{wi}$  is initial irreducible water saturation, %;  $S_{wim}$  is irreducible water saturation of matrix system in the initial state, %;  $S_{wif}$  is irreducible water saturation of fracture system in the initial state, %.

The initial oil saturation can be calculated by  $1 - S_{wi}$ .

Considering the compressibility of fracture system, for each new reservoir pressure  $p_{i+1}$ , the fracture porosity  $\varphi_f$  and fracture permeability  $k_f$  are calculated through the equation proposed by Jone (Jones 1975).

$$\frac{\varphi_{fi+1}}{\varphi_{fi}} = \left( \frac{k_{fi+1}}{k_{fi}} \right)^{1/3} = \frac{\log p_{i+1} - \log p_h}{\log p_i - \log p_h} \tag{9}$$

where  $\varphi_f$  is the porosity of fracture system, %;  $k_f$  is permeability of fracture system, mD.

Calculate partition coefficient of step  $i + 1$

$$v_{i+1} = \frac{\varphi_{fi+1}}{\varphi_{fi+1} + \varphi_{mi+1}} \tag{10}$$

where

$$\varphi_{mi+1} = (1 - \varphi_{fi+1})\varphi_b \tag{11}$$

$\varphi_b$  is matrix porosity related to the volume of matrix system, which is assumed to be a constant value.  $\varphi_m$  is porosity of matrix related to the total volume of matrix and fracture systems. Since fracture porosity changes with pressure, the value of  $\varphi_m$  also changes.

The pressure drop is taken at a certain interval and calculated in several steps. For a new pressure value, assuming that the cumulative oil production in step  $i + 1$  is  $(N_p)_{i+1}$ , calculate oil saturation  $S_o$  and gas saturation  $S_g$ . Calculate fracture system oil saturation  $S_{of}$  based on the previously calculated matrix system oil saturation  $S_{om}$ .

$$(S_o)_{i+1} = \left[ 1 - \frac{(N_p)_{i+1}}{N} \right] \frac{B_o}{B_{ob}} (1 - S_{wc}) \tag{12}$$

$$(S_g)_{i+1} = 1 - (S_o)_{i+1} - S_{wc} \tag{13}$$

$$(S_{of})_{i+1} = \frac{(S_o)_{i+1} - (S_{om})_{i+1}(1 - v_{i+1})}{v_{i+1}} \quad (14)$$

where  $S_o$  is total oil saturation, %;  $S_{om}$  is oil saturation of matrix system, %;  $S_{of}$  is oil saturation of fracture system, %.

Calculate instantaneous production gas–oil ratio  $R$

$$(R)_{i+1} = \left( R_s + \frac{B_o \mu_o k_{rg}}{B_g \mu_g k_{ro}} \right)_{i+1} \quad (15)$$

where  $\mu_o$  is oil viscosity, mPa·s;  $\mu_g$  is gas viscosity, mPa·s;  $k_{rg}$  is relative permeability of gas phase;  $k_{ro}$  is relative permeability of oil phase.

Next, calculate relative permeability of oil and gas. If there are available experimental data, use the results of experimental data to substitute into calculation; if not, calculate  $k_{rg}$ ,  $k_{ro}$  according to the following formula

$$(k_{rg})_{i+1} = k_{rg}^0 S_{i+1} \quad (16)$$

$$(k_{ro})_{i+1} = k_{ro}^0 (1 - S_{i+1}) \quad (17)$$

Substituting calculation results above into Eq. (6) to calculate the increase in oil production in step  $i + 1$ , add it to the cumulative oil production in step  $i$ , and calculate the cumulative oil production in step  $i + 1$

$$(N_p)_{i+1} = (N_p)_i + \Delta N_p \quad (18)$$

Compare calculation result of above formula with the hypothetical one. If the accuracy is satisfied, proceed to next step; if not, then reset hypothetical value and repeat the above calculation procedure until accuracy is satisfied.

So far, the relationship between cumulative oil production and pressure has been obtained. The following steps permit computation of oil recovery as a function of time.

To get the relationship between oil production and time, oil production index must be introduced

$$J_{i+1} = J_1 \frac{(k_{ro})_{i+1} (\mu_o B_o)_1}{R_{res} (k_{ro})_1 (\mu_o B_o)_{i+1}} \quad (19)$$

where  $R_{res}$  is resistance correction coefficient, which is obtained from experimental results in the previous section. Fit the relationship between resistance and pressure as a formula and substitute it into  $J$  for calculation.

Calculate oil production rate

$$(q_o)_{i+1} = J_{i+1} (p_{i+1} - p_{wf,i+1}) \quad (20)$$

where  $J$  is oil production index,  $m^3/(d \cdot MPa^{-1})$ ;  $q_o$  is oil production rate,  $m^3/d$ ;  $p_{i+1}$  is reservoir pressure at step  $i + 1$ , MPa;  $p_{wf}$  is production well pressure, MPa.

Calculate the annual output decline rate and time increment from step  $i$  to step  $i + 1$  by combining the previously calculated cumulative oil production increment  $(\Delta N_p)_{i+1}$  in step  $i + 1$

$$a_{i+1} = 365 \left[ \frac{(q_o)_i - (q_o)_{i+1}}{(\Delta N_p)_{i+1}} \right] \quad (21)$$

where  $a$  is annual decline rate of oil production, %.

Calculate the time increment from  $q_i$  to  $q_{i+1}$

$$(\Delta t)_{i+1} = \ln \left( \frac{q_{oi}}{q_{oi+1}} \right) / a_{i+1} \quad (22)$$

Calculate cumulative time

$$t_{i+1} = t_i + \Delta t_{i+1} \quad (23)$$

where  $t$  is accumulated production time, d;  $\Delta t$  is increment of production time, d.

For each new pressure, repeat the above calculation procedure until reservoir abandoned pressure is reached. So far, relationship between each variable and time is obtained.

For unsaturated oil reservoirs in the initial state and gradually becoming saturated during depletion production, the calculation of cumulative oil production needs to combine the material balance equations of both saturated oil reservoirs and unsaturated ones and be calculated as follows:

1. When the average reservoir pressure is higher than bubble point, the oil production should be calculated by Eq. (3).
2. When the average reservoir pressure is lower than bubble point, the cumulative oil production should be calculated from:

$$(N_p)_{Total,i+1} = N \left\{ \left[ 1 - \left( \frac{N_p}{N} \right)_b \left( \frac{N_p}{N} \right)_{i+1} \right] \right\} + N \left( \frac{N_p}{N} \right)_b \quad (24)$$

where  $(N_p)_{Total,i+1}$  is the total cumulative oil production when the average reservoir pressure is lower than the bubble point at step  $i + 1$ ;  $N$  is the original oil-in-place;  $(N_p)_{i+1}$  is determined by Eq. (18);  $(N_p/N)_b$  is the recovery at bubble point pressure.

## Example calculation

Taking the depletion exploitation of gas-bearing tight oil reservoirs as an example, compare effects of dissolved gas on production of oil reservoirs with different lithologies. Assuming that the original oil-in-place is  $6503.4 \times 10^4$ t, the initial formation pressure is 18 MPa, the abandoned pressure is 2 MPa, the bubble point pressure is 10.5 MPa, the recoverable reserves is  $2 \times 10^5$ t, the crude oil volume factor is 1.247,



and the original dissolved gas–oil ratio is  $92\text{m}^3/\text{t}$ . The irreducible water saturation is 25%, the gas volume coefficient under original condition is 0.0092, and the pressure drop step size is 0.5 MPa. The resistance coefficient of dissolved gas is calculated using the experimental results of porous flow resistance of central Sichuan sandstone and central Sichuan limestone, respectively. The calculation results are shown in Figs. 9 and 10.

From the oil production graphs of sandstone and limestone reservoirs, it can be seen that the resistance generated by separation of dissolved gas has a significant impact on oil production of both sandstone and limestone reservoirs. The lower the permeability, the greater the impact. It is obvious that after the inflection point, production drops sharply, and the downward trend of the curve with lower permeability is steeper. Compared with different lithologies, limestone reservoirs are more affected by dissolved gas resistance. It is easy to see from

the daily production curves that under the same conditions, the curve after the degassing point of limestone reservoirs drops steeper than that of sandstone reservoirs. The cumulative production of sandstone reservoirs is significantly smoother than limestone reservoirs, the latter of which has an obvious inflection point, indicating that the porous flow resistance has a greater impact on limestone reservoirs. The cumulative production curves combined with the experimental ones indicate that the heterogeneity of the limestone reservoir is stronger. Furthermore, the fluid storage space and the flow space do not match, which means that the phase interface produced by the separated dissolved gas probably blocks the limestone throat causing increased resistance and affecting production capacity. Hence, the production pressure should be kept above the bubble point when exploiting limestone reservoirs.

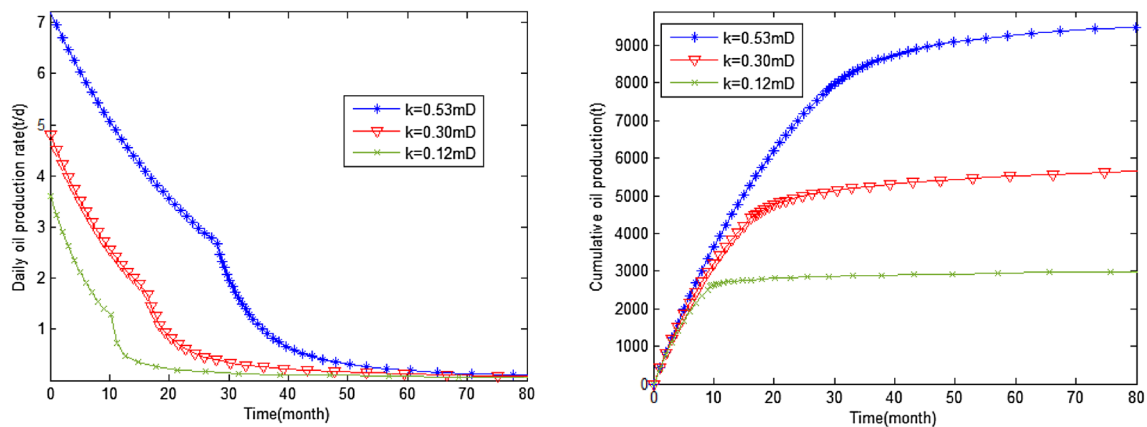


**Fig. 9** Daily oil production (left) and cumulative oil production (right) of sandstone reservoirs

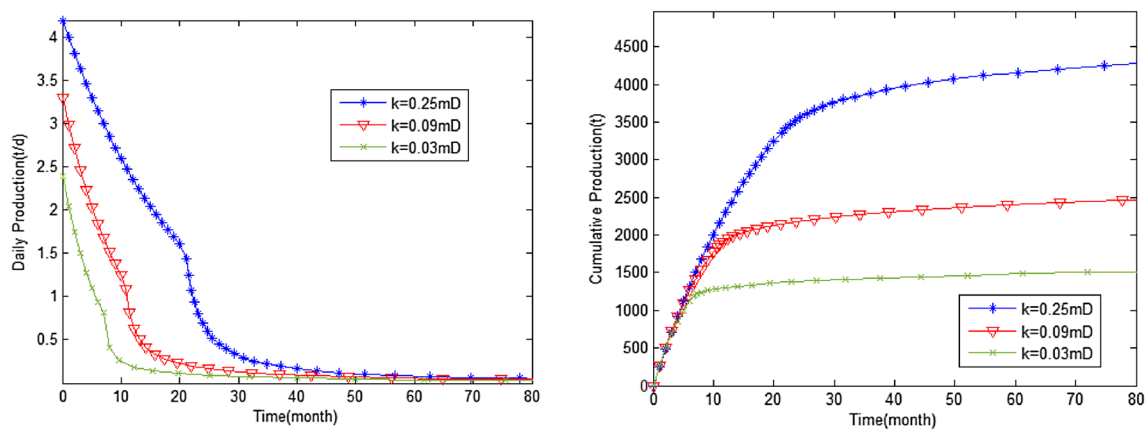


**Fig. 10** Daily oil production (left) and cumulative oil production (right) of limestone reservoirs

## Conclusions

- (1) For sandstone formations in Ordos and Sichuan Basin, resistance gradients are not much different and have similar variation laws; while resistance gradient of limestone is much larger than that of sandstone under the same conditions. It shows that pore structure has a great influence on resistance gradient. If fluid storage space does not match flow space, resistance gradient will rise steeply.
- (2) The PVT characteristics in nanoscale pores are different from that measured in high-temperature and high-pressure sampler. Only when pressure is lower than a certain value of the bubble point pressure of the gas-containing crude oil measured in high-temperature and pressure sampler will dissolved gas begin to separate out and produce resistance.
- (3) When exploiting tight limestone reservoirs, it should be kept above bubble point pressure; while exploiting tight sandstone reservoirs, production pressure can be reduced to a certain range below the bubble point pressure when permeability is high, and when permeability is low, it should be kept above bubble point pressure.

## Open access

This article is licensed under a Creative Commons Attribution 4.0 International License, which permits use, sharing, adaptation, distribution and reproduction in any medium or format, as long as you give appropriate credit to the original author(s) and the source, provide a link to the Creative Commons licence, and indicate if changes were made. The images or other third party material in this article are included in the article's Creative Commons licence, unless indicated otherwise in a credit line to the material. If material is not included in the article's Creative Commons licence and your intended use is not permitted by statutory regulation or exceeds the permitted use, you will need to obtain permission directly from the copyright holder. To view a copy of this license, visit <http://creativecommons.org/licenses/by/4.0/>.

**Funding** This work was funded by the National Science and Technology Major Project of China (Grant No. 2017ZX05013-001 and 2017ZX05069-003) and China National Petroleum Corporation Scientific Research and Technology Development Project (KT2017-19-05-1).

**Availability of data and material** The data that support the findings of this study will be available from the corresponding author upon request.

## Declarations

**Conflict of interest** On behalf of all the co-authors, the corresponding author states that there is no conflict of interest.

**Open Access** This article is licensed under a Creative Commons Attribution 4.0 International License, which permits use, sharing, adaptation, distribution and reproduction in any medium or format, as long as you give appropriate credit to the original author(s) and the source, provide a link to the Creative Commons licence, and indicate if changes were made. The images or other third party material in this article are included in the article's Creative Commons licence, unless indicated otherwise in a credit line to the material. If material is not included in the article's Creative Commons licence and your intended use is not permitted by statutory regulation or exceeds the permitted use, you will need to obtain permission directly from the copyright holder. To view a copy of this licence, visit <http://creativecommons.org/licenses/by/4.0/>.

## References

- Abusahmin BS, Karri RR, Maini BB (2017) Influence of fluid and operating parameters on the recovery factors and gas oil ratio in high viscous reservoirs under foamy solution gas drive [J]. *Fuel* 197:497–517
- Akin S, Kovsky AR (2002) Heavy-oil solution gas drive: a laboratory study[J]. *J Petrol Sci Eng* 35(1):33–48
- Ali M, Jarni HH, Aftab A et al (2020) Nanomaterial-based drilling fluids for exploitation of unconventional reservoirs: a review[J]. *Energies* 13(13):3417
- Arora P, Kovsky AR (2003) A mechanistic modeling and experimental study of solution gas drive[J]. *Transp Porous Media* 51(3):237–265
- Bora R, Maini BB, Chakma A (2000) Flow visualization studies of solution gas drive process in heavy oil reservoirs using a glass micromodel[J]. *SPE Reservoir Eval Eng* 3(3):224–229
- Chatenever A, Indra MK, Kyte JR (1959) Microscopic observations of solution gas-drive behavior[J]. *J Petrol Technol* 11(6):13–15
- Chen WX, Zhang ZB, Liu QJ et al (2018) Experimental investigation of oil recovery from tight sandstone oil reservoirs by pressure depletion[J]. *Energies* 11:2667
- Danesh A, Peden JM, Krinis D, et al (1987) Pore level visual investigation of oil recovery by solution gas drive and gas injection[C], *Spe Technical Conference & Exhibition*.
- Dominguez A, Bories S, PratGas M (2000) cluster growth by solute diffusion in porous media. Experiments and automaton simulation on pore network[J]. *Int J Multiph Flow* 26:1951–1979
- Annual ENERGY outlook 2020. EIA, Major U S. <https://www.eia.gov/todayinenergy/>. 2020.
- Gao JX, Yao YD, Liu Z et al (2021) A model for nitrogen injection in horizontal wells of tight oil reservoirs[J]. *Energy Sour Part A-Recovery Util Environ Eff*. <https://doi.org/10.1080/15567036.2021.1903622>
- Guo QL, Wang SJ, Chen XM et al (2018) Assessment on tight oil resources in major basins in China[J]. *J Asian Earth Sci* 178:52–63. <https://doi.org/10.1016/j.jseaes.2018.04.039>
- Guo RL, Xie QC, Qu XF et al (2020) Fractal characteristics of pore-throat structure and permeability estimation of tight sandstone reservoirs: a case study of Chang 7 of the upper triassic yanchang formation in Longdong area, Ordos Basin, China[J]. *J Pet Sci Eng* 184:106555

- Jones J (1975) A laboratory study of the effects of confining pressure on fracture flow and storage capacity in carbonate rocks[J]. *J Pet Technol* 12:55
- Jones SR (2016) Producing-gas/oil-ratio behavior of multifractured horizontal wells in tight oil reservoirs[J]. *SPE Reserv Eval Eng* 20:589–601
- Lago M, Huerta M, Gomes R (2002) Visualization study during depletion experiments of venezuelan heavy oils using glass micromodels[J]. *J Can Pet Technol*. <https://doi.org/10.2118/02-01-03>
- Li P, Zheng M, Bi H et al (2017) Pore throat structure and fractal characteristics of tight oil sandstone: a case study in the Ordos Basin, China. *J Petrol Sci Eng* 149:665–674
- Li Z, Wu S, Xia D et al (2018) An investigation into pore structure and petrophysical property in tight sandstones: a case of the Yanchang Formation in the southern Ordos Basin, China[J]. *Mar Pet Geol* 97:390–406
- Li B, Wang XZ, Liu HQ et al (2020) Tight carbonate microstructure and its controls: a case study of Lower Jurassic Da'anzhai Member, central Sichuan Basin. *Acta Geol Sin* 94(2):305–321. <https://doi.org/10.1111/1755-6724.14307>
- Lin W, Li XZ, Yang ZM et al (2018) A new improved threshold segmentation method for scanning images of reservoir rocks considering pore fractal characteristics[J]. *Fractals* 26(2):1840003
- Lin W, Xiong SC, Liu Y et al (2021) Spontaneous imbibition in tight porous media with different wettability: pore-scale simulation[J]. *Physics of Fluids* 33:032013
- Lu T, Li ZM, Li SY et al (2016) Enhanced heavy oil recovery after solution gas drive by water flooding[J]. *J Petrol Sci Eng* 137:113–124
- Maini BB (1999) Foamy oil flow in primary production of heavy oil under solution gas drive[C]. *Spe Technical Conference & Exhibition*. Society of Petroleum Engineers.
- Moulu JC (1989) Solution-gas drive: experiments and simulation[J]. *J Petrol Sci Eng* 2:379–386
- Nithiwat S, Turgay E, Russell TJ (2017) Compositional simulation of hydraulically fractured tight formation considering the effect of capillary pressure on phase behavior[J]. *SPE J* 22:1046–1063
- Nojabaei B, Johns RT, Chu L (2013) Effect of capillary pressure on phase behavior in tight rocks and shales[J]. *SPE Reserv Eval Eng* 16(3):281–289
- Orozco D, Aguilera R (2018) Material balance forecast of huff-and-puff gas injection in multiporosity shale oil reservoirs[J]. *SPE* 189783
- Qiao JC, Zeng JH, Jiang S et al (2020) Role of pore structure in the percolation and storage capacities of deeply buried sandstone reservoirs: a case study of the Junggar Basin, China[J]. *Mar Pet Geol* 113:104129
- Qin Y, Yao SP, Xiao HM et al (2021) Pore structure and connectivity of tight sandstone reservoirs in petroleum basins: a review and application of new methodologies to the Late Triassic Ordos Basin, China[J]. *Mar Pet Geol* 129:105084
- Sheikha H, Darvish MP (2012) Micro bubbles in solution-gas drive in heavy oil: their existence and importance[J]. *Transp Porous Med* 93:495–516
- Shen WJ, Li XZ, Ma TR et al (2021) High-pressure methane adsorption behavior on deep shales: experiments and modeling[J]. *Phys Fluid* 33(6):063103
- Smith GE (1988) Fluid flow and sand production in heavy-oil reservoirs under solution-gas Drive[J]. *Spe Prod Eng* 3(2):169–180
- Song ZJ, Song YL, Li YZ et al (2020) A critical review of CO<sub>2</sub> enhanced oil recovery in tight oil reservoirs of North America and China[J]. *Fuel* 276:118006
- Song Y, Song Z, Feng D et al (2020) Phase behavior of hydrocarbon mixture in shale nanopores considering the effect of adsorption and its induced critical shifts[J]. *Indus Eng Chem Res* 59:8374–8382
- Stewart CR, Hunt EB, Schneider FN et al (1954) The role of bubble formation in oil recovery by solution gas drives in limestones[J]. *J Petrol Technol* 5(12):21–28
- Wang YJ, Tong M, Sun YH et al (2019) Reservoir characteristics of Da'anzhai shell limestone tight oil in Sichuan Basin. *Acta Petrolei Sinica* 40(1):46–59
- Wang Q, Yang SL, Glover PWJ et al (2020) Effect of pore-throat microstructures on formation damage during miscible CO<sub>2</sub> flooding of tight sandstone reservoirs. *Energy Fuels* 34(4):4338–4352
- Wu CM, Guo ZN, Tang FP et al (2014) Early Exploitation characteristics of lucaogou tight oil of Permian in Jimusaer Sag, Junggar Basin[J]. *Xinjiang Pet Geol* 35(5):570–573
- Xiao QH, Wang ZY, Yang ZM et al (2018) Porous flow characteristics of solution-gas drive in tight oil reservoirs[J]. *Open Phys* 16(1):412–418
- Yan BC, Wang YH, Killough JE (2017) A fully compositional model considering the effect of nanopores in tight oil reservoirs[J]. *J Pet Sci Eng* 152:675
- Yang ZM, Guo HK, Liu XW et al (2017) Micro-pore structure test and physical simulation technology of low permeability-tight reservoirs. *Petroleum industry press*, Beijing
- Zhang ML, Mei HY, Li M et al (2002) A phase equilibrium model in volatile petroleum system under consideration of capillary pressure. *China Offshore Oil Gas (Geol)* 16(5):48–51
- Zhang MS, Sang Q, Gong HJ et al (2018) Effect of depletion rate on solution gas drive in shale[J]. *Iop Conf*. <https://doi.org/10.1088/1755-1315/108/3/032078>
- Zhang WK, Shi ZJ, Tian YM (2020) An improved method to characterize the pore-throat structures in tight sandstone reservoirs: combined high pressure and rate-controlled mercury injection techniques[J]. *Energy Explor Exploit* 0(0):1–24.
- Zhou NW, Lu SF, Wang M et al (2021) Limits and grading evaluation criteria of tight oil reservoirs in typical continental basins of China[J]. *Pet Explor Dev* 48(5):1–11
- Zhu RK, Zou CN, Wu SY et al (2019) Mechanism for generation and accumulation of continental tight oil in China[J]. *Oil Gas Geol* 40(6):1168–1184

**Publisher's Note** Springer Nature remains neutral with regard to jurisdictional claims in published maps and institutional affiliations.